Two-step homogenization of spatiotemporal metasurfaces using an eigenmode-based approach

Puneet Garg,[1,2,*] Aristeidis G. Lamprianidis,[1,2] Sydur Rahman,[1] Nikolaos Stefanou,[3] Evangelos Almpanis,[3,4] Nikolaos Papanikolaou,[4] Barbara Verfürth,[5] and Carsten Rockstuhl[1,2,6]

[1] *Institute of Theoretical Solid State Physics, Karlsruhe Institute of Technology, Kaiserstr. 12, 76131 Karlsruhe, Germany*
[2] *Max Planck School of Photonics, Jena, 07745 Germany*
[3] *Section of Condensed Matter Physics, National and Kapodistrian University of Athens, Panepistimioupolis, GR-157 84 Athens, Greece*
[4] *Institute of Nanoscience and Nanotechnology, NCSR "Demokritos," Patriarchou Gregoriou and Neapoleos Str., Ag. Paraskevi, GR-153 10 Athens, Greece*
[5] *Institut für Numerische Simulation, Universität Bonn, Friedrich-Hirzebruch-Allee 7, 53115 Bonn*
[6] *Institute of Nanotechnology, Karlsruhe Institute of Technology, Kaiserstr. 12, 76131 Karlsruhe, Germany*
[*] *puneet.garg@kit.edu*

Abstract: Metamaterials are a fascinating class of photonic materials since they allow us to control optical responses (largely) at will. Besides being an intellectual challenge, adding time variations into spatial metamaterials increases the degrees of freedom to tune their effective response, which motivates their exploration. However, to exploit such materials in the future design of functional devices, we may wish to treat them at the effective level to avoid considering all the mesoscopic details. To permit such effective treatment, we describe here an eigenmode-based approach to homogenize spatiotemporal metamaterials composed of a periodic arrangement of scatterers made from a time-varying material. Practically, we consider the periodic arrangement of spheres within one layer. In our two-step homogenization scheme, we first temporally homogenize that metasurface using the eigenmodes of the bulk time-varying material. Following this, we perform spatial homogenization by inverting the Fresnel coefficients of a slab made from a stationary material. These steps effectively describe the optical response of the spatiotemporal metasurface as a homogeneous slab. We validate our results by comparing the optical observables, i.e., reflectivity and transmissivity, of the metasurface with those of the homogenized slab, and we assess the limitations of the homogenization.

1. Introduction

Metamaterials are artificial photonic materials made from a periodic arrangement of basic constituent units called meta-atoms [1, 2]. These artificial materials have been extensively explored due to their degrees of freedom in tailoring light-matter interactions [3]. Metamaterials can be employed to achieve extreme effective material parameters, such as negative and near-zero permittivity and permeability [4–6]. These extraordinary effective properties are made possible by spatial inhomogeneities in three dimensions (3D) that constitute the metamaterials. Specifically, the local resonances of the meta-atoms drive such extreme behavior [7]. Moreover, metamaterials exhibit many exotic optical phenomena inaccessible to natural materials, including invisibility cloaking [8], superlensing [9, 10], perfect absorption [11, 12], artificial magnetism [13], negative refraction [14], and giant optical activity [15], among others.

Recently, time-varying metamaterials have garnered significant attention within the scientific community [16, 17]. The introduction of temporal inhomogeneity in metamaterials has opened up new avenues for controlling their effective properties in four dimensions (4D) [18–20]. These temporally modulated materials exhibit an immense potential to advance the applications of metamaterials. Notable findings in the realm of time-varying metamaterials include temporal reflection and refraction [21, 22], frequency conversion [23], momentum bandgap [24–26], non-reciprocal light propagation [27], power combining of waves [28], antireflection temporal coatings [29], temporal aiming [30], optical isolators [31], synthetic axion response [32], parametric amplification [33,34], and more [35,36]. Recent experimental advances in modulating material parameters as a function of time have further fueled research on temporal metamaterials. Epsilon-near-zero (ENZ) materials, in particular, have emerged as promising candidates to achieve such time-varying material parameters [37–39]. These ENZ materials hold the potential to facilitate ultrafast modulation of material properties in time with reasonably high strength [40].

In this contribution, our focus lies on the homogenization of spatiotemporal metamaterials (MMs) [41–44]. As the term implies, homogenization is a process aimed at approximating the optical response of inhomogeneous materials with homogeneous media [45]. These homogenized media are characterized optically by effective material parameters [4, 46]. Homogenization requires the spatial inhomogeneity that forms the MM to be smaller, or ideally much smaller than the operational wavelength, and we extend a similar requirement to the temporal domain.

So far, many works have addressed the homogenization of time-varying MMs. For instance, in [47], an effective description of a temporal multi-stepped system with a single temporal interface was demonstrated. The homogenization of temporal multi-stepped systems in acoustics is discussed in [48]. Nonlocal homogenization theories for temporal MMs were proposed in [49,50]. The homogenization of spatiotemporal MMs, considering traveling-wave modulation of material parameters, was explored in [42] and [43]. Additionally, [41] discusses the homogenization of bulk systems multi-stepped in both space and time. Furthermore, [44] considers the homogenization of spatiotemporally modulated wire media. Inspired by these works, we develop a homogenization theory for spatiotemporal metasurfaces (MSs) [20,51]. Our interest in MSs is motivated by their ability to relax the requirement of temporal modulation in extended space [52]. Compared to many other prior contributions, we stress that the geometry considered here is a thin layer of a 3D spatially structured material that changes its properties in time.

The homogenization theory presented in this article relies on the eigenmodes of bulk time-varying media. We employ the method introduced in [53] to calculate, first, the eigenmodes of bulk time-varying media with permittivity $\varepsilon(t)$. Subsequently, we analyze these eigenmodes to identify the spectral region where temporal homogenization can be applied. Additionally, we demonstrate how the effective permittivity of the corresponding homogenized media can be determined using these eigenmodes. Once the effective permittivity of the bulk time-varying medium is retrieved, we validate our homogenization scheme by comparing the optical observables (reflectivity, transmissivity, and absorptivity) of time-varying bulk media that forms a temporal slab with those of the corresponding homogenized media. To calculate the optical observables of the bulk time-varying media that forms a temporal slab, we utilize the transfer matrix-based method proposed in [54].

Afterward, we extend the versatility of the proposed homogenization method by applying it to a spatiotemporal MS. We consider an MS composed of spheres made from a material characterized by a time-varying permittivity $\varepsilon(t)$. To homogenize such a system in space and time, we propose a two-step homogenization scheme. In the first step, we temporally homogenize the MS using the eigenmodes of the bulk system with permittivity $\varepsilon(t)$. This initial step simplifies the considered system to a time-invariant MS of spheres. In the second step, we proceed to spatially homogenize the time-invariant MS by describing it as a spatially homogeneous slab. For this spatial homogenization, we employ the well-known method of inverting the Fresnel

coefficients of a slab [6,55]. This inversion yields, finally, the effective material parameters of the slab. To assess the ability of our two-step homogenization, we compare the optical observables (reflectivity and transmissivity) of the spatiotemporal MS with those of the homogenized slab. To calculate the optical observables of the spatiotemporal MS, we utilize the T-matrix-based method introduced in [20]. It's worth noting that the theory developed in our article can be applied to systems with any arbitrary shape of the time-periodic permittivity profile $\varepsilon(t)$.

2. Theory

2.1. Eigenmodes of bulk time-varying media

We examine the dynamics of an electromagnetic wave in a bulk, linear, isotropic, dispersionless, non-magnetic, and source-free time-varying medium. We assume the permittivity ε of the medium to be a periodic function of time with a time-period T_m (corresponding to a modulation frequency $\omega_\mathrm{m} = 2\pi/T_\mathrm{m}$). This periodicity is expressed as $\varepsilon(t + T_\mathrm{m}) = \varepsilon(t)$. Additionally, we represent $\varepsilon(t) = 1 + \chi(t)$, where $\chi(t)$ is the time-periodic electrical susceptibility of the medium, satisfying $\chi(t + T_\mathrm{m}) = \chi(t)$. In the frequency domain, the wave equation governing the electric field $\tilde{\mathbf{E}}(\mathbf{r}, \omega)$ within the medium can be expressed as [53, Eq. 4]

$$\nabla \times \nabla \times \tilde{\mathbf{E}}(\mathbf{r}, \omega) = k_0^2(\omega) \left[\tilde{\mathbf{E}}(\mathbf{r}, \omega) + \int_{-\infty}^{\infty} \tilde{\chi}(\omega - \omega') \tilde{\mathbf{E}}(\mathbf{r}, \omega') \mathrm{d}\omega' \right], \tag{1}$$

where $k_0(\omega) = \omega/c_0$ with c_0 being the speed of light in vacuum, and $\tilde{\chi}(\omega)$ is the Fourier transform of the time-varying electric susceptibility $\chi(t)$ [56]. Note that the convolution integral on the right-hand side of Eq. (1) implies coupling of Maxwell's equations in frequency. This coupling signifies that within media having time-dependent electrical susceptibility, a monochromatic electric field excitation with frequency ω results in a polychromatic polarization density [20].

Next, to find the eigenmodes of the time-varying medium, we use the following ansatz to solve Eq. (1) [53, Eq. 5]

$$\tilde{\mathbf{E}}(\mathbf{r}, \omega) = \sum_i A_{\kappa_i} S_{\kappa_i}(\omega) \mathbf{F}(\kappa_i \mathbf{r}), \tag{2}$$

where A_{κ_i} are complex amplitudes, and $S_{\kappa_i}(\omega)$ and $\mathbf{F}(\kappa_i \mathbf{r})$ are the spectral and spatial parts of the eigenmodes, respectively. Substituting the ansatz of Eq. (2) in Eq. (1), we find that $\mathbf{F}(\kappa_i \mathbf{r})$ is a solution of the vector Helmholtz equation with eigenwavenumber κ_i [57]. Further, $S_{\kappa_i}(\omega)$ can be numerically calculated using the eigenvalue equation (see the Supplementary Material; Sec 1) [53, Eqs. 8–11]

$$\hat{\mathbf{K}}(\omega) \cdot \mathbf{S}_{\kappa_i}(\omega) = \kappa_i^2(\omega) \mathbf{S}_{\kappa_i}(\omega), \text{ with} \tag{3a}$$

$$\hat{\mathbf{K}}(\omega) = \hat{\mathbf{k}}_\mathbf{0}^\mathbf{2} \cdot (\hat{\mathbf{I}} + \hat{\tilde{\boldsymbol{\chi}}}), \tag{3b}$$

$$\mathbf{S}_{\kappa_i}(\omega) = [S_{\kappa_i}(\omega_{-N}), S_{\kappa_i}(\omega_{-N+1}), ..., S_{\kappa_i}(\omega_N)]^\mathrm{T}, \text{and} \tag{3c}$$

$$\hat{\mathbf{k}}_\mathbf{0} = \mathrm{diag}[k_0(\omega_{-N}), k_0(\omega_{-N+1}), ..., k_0(\omega_N)]. \tag{3d}$$

Here, κ_i^2 represent the eigenvalues, and $\mathbf{S}_{\kappa_i}(\omega)$ denote the corresponding eigenvectors of the eigenvalue equation (Eq. (3a)). Additionally, $\hat{\mathbf{I}}$ is the identity matrix, and $\hat{\tilde{\boldsymbol{\chi}}}$ is the electrical susceptibility matrix with elements $\tilde{\chi}_{jl} = \tilde{\chi}(\omega_j - \omega_l)$, where $\omega_j = \omega + j\omega_\mathrm{m}$ and $j \in [-N, N]$. Here, N is a suitably chosen integer, and it is essential to set N sufficiently large for numerical convergence. Solving Eq. (3a) yields $2N + 1$ eigenvalues and their corresponding eigenvectors. These are enumerated with the index $i \in [-N, N]$. Furthermore, the eigenvectors are arranged in ascending order based on the eigenvalues κ_i^2.

Finally, in the time domain, the i^{th} eigenmode of the time-varying media at eigenfrequency ω with eigenwavenumber κ_i can be written as

$$\mathbf{E}_i(\mathbf{r},t) = \sum_{j=-N}^{N} S_{\kappa_i}(\omega_j)\mathbf{F}(\kappa_i\mathbf{r})e^{-\mathrm{i}(\omega+j\omega_\mathrm{m})t}\,. \tag{4}$$

2.2. Homogenizability conditions of bulk time-varying media

In this subsection, we explore the homogenizability conditions of bulk time-varying systems. Fulfilling these conditions is essential for the validity of the temporal effective medium description.

2.2.1. Monochromaticity of eigenmodes

As evident from Eq. (4), the eigenmodes of bulk time-varying media are generally polychromatic [58]. However, a system lacking a time-varying electrical permittivity only supports monochromatic eigenmodes. Our objective here is to homogenize time-varying media. The homogenization procedure involves approximating time-varying media (with time-periodic permittivity $\varepsilon(t)$) by effective time-invariant media (with time-invariant permittivity $\tilde{\varepsilon}_\mathrm{eff}$). This approximation must ensure that the dynamics of electromagnetic fields in both media are indistinguishable, at least up to a notable degree. Therefore, for time-varying media to be homogenizable, it is crucial that its eigenmodes are quasi-monochromatic.

Here, we examine the monochromaticity of the eigenmodes of the time-varying media numerically. To check whether the time-varying media supports quasi-monochromatic eigenmodes at eigenfrequency ω, we first calculate its eigenvectors $\mathbf{S}_{\kappa_i}(\omega)$ with $i \in [-N, N]$ (see Eq. (3a)). Next, we search for that eigenvector which has the maximal value of the quantity $|S_{\kappa_i}(\omega_0)|^2$ (see Eq. (3c)). Note that numerically $\omega_0 = \omega$, since $\omega_j = \omega + j\omega_\mathrm{m}$. Let us denote that eigenvector as $\mathbf{S}_k$ with eigenvalue $k^2 = \kappa_p^2$ for some $p(\omega) \in [-N, N]$. Since $\mathbf{S}_{\kappa_i}$ are normalized eigenvectors, the closeness of the numerical value of $|S_k(\omega_0)|^2$ to 1 would imply quasi-monochromaticity of the eigenvector $\mathbf{S}_k$. Therefore, we define the monochromaticity $M\%$ of the eigenvector $\mathbf{S}_k$ at frequency ω as

$$M\%(\omega) = 100 \times |S_k(\omega_0)|^2\,. \tag{5}$$

Additionally, we must ensure that all other eigenvectors, apart from $\mathbf{S}_k$, have a vanishing value of $|S_{\kappa_i}(\omega_0)|^2$. This condition is crucial for establishing a one-to-one correspondence between frequency and wavenumber, similar to an isotropic time-invariant medium (refer to Eq. (2)). This requirement can be met by ensuring that the numerical value of the quantity $Q(\omega) = \left(\sum_{i=-N}^{N} |S_{\kappa_i}(\omega_0)|^2\right) - |S_k(\omega_0)|^2$ is close to zero.

Once monochromaticity and the one-to-one correspondence of frequency and wavenumber are ensured, the time-varying media can be approximated as effective time-invariant media with wavenumber k for frequency ω (refer to Eq. (2)). Consequently, the effective permittivity $\tilde{\varepsilon}_\mathrm{eff}$ of the corresponding homogenized media can be expressed as

$$\tilde{\varepsilon}_\mathrm{eff}(\omega) = \frac{k^2}{k_0^2(\omega)}\,. \tag{6}$$

2.2.2. Constraints on frequency

As mentioned earlier, temporal homogenization involves approximating time-periodic media with effective time-invariant media. Naturally for such homogenization to be possible, we require the modulation frequency ω_m to be greater than the excitation frequency ω of the fields, i.e., $\omega_\mathrm{m} > \omega$. This is because, for a system to be homogenizable, it is necessary that the excitation

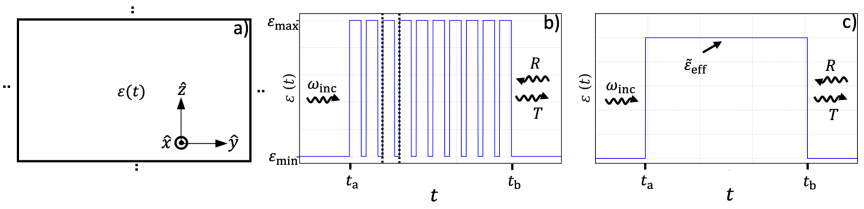

Fig. 1. a) Illustration of a bulk time-periodic medium with permittivity $\varepsilon(t)$, b) variation of the permittivity ε of the medium shown in a) as a function of time t when a temporal slab is considered. c) Permittivity of the homogenized medium corresponding to the time-periodic medium in a)–b). Here, at $t = t_a$ and t_b in b) and c) temporal interfaces exist so that a slab is formed. Further, the black-dotted lines b) enclose one period of the rectangular wave.

frequency is unable to detect the temporal variations of the media [49]. This is implied if these variations are fast enough compared to the frequency of the involved electromagnetic field.

In particular, we know that in the time domain, the general solution of Eq. (1) for the electric field $\mathbf{E}(\mathbf{r}, t)$ is written as [24, 49]

$$\mathbf{E}(\mathbf{r}, t) = \sum_{j=-N}^{N} \tilde{\mathbf{E}}(\mathbf{r}, \omega_j) e^{-\mathrm{i}(\omega + j\omega_\mathrm{m})t} \,. \tag{7}$$

Further, let us denote the field inside the homogenized media as $\mathbf{E}_\mathrm{h}(\mathbf{r}, t)$. Due to monochromaticity (see Subsection 2.2.1), we need $\mathbf{E}_\mathrm{h}(\mathbf{r}, t) = \tilde{\mathbf{E}}(\mathbf{r}, \omega) e^{-\mathrm{i}\omega t}$. Moreover, as the effective media cannot detect fast temporal variations of the system, we expect $\mathbf{E}_\mathrm{h}(\mathbf{r}, t)$ to be the slowest component of $\mathbf{E}(\mathbf{r}, t)$ (see Eq. (7)). Therefore, homogenizability requires $\tilde{\mathbf{E}}(\mathbf{r}, \omega) e^{-\mathrm{i}\omega t}$ to be the slowest component of $\mathbf{E}(\mathbf{r}, t)$. This is possible only if $|\omega| < 0.5\omega_\mathrm{m}$. In other words, the excitation frequency ω must lie in the first temporal Brillouin zone of the temporal lattice characterized by the modulation frequency ω_m. This condition is the temporal analog of the condition for spatial homogenization mentioned in [59, 60].

3. Results

In this section, we present the applications of the temporal homogenization method described above. Initially, we show the temporal homogenization of bulk time-varying media. Then, we apply the method to spatiotemporal MSs made from time-varying dielectric spheres.

3.1. Homogenization of bulk time-varying media

Here, we explore the homogenization of bulk time-varying media. As shown in Fig. 1(a), we consider a spatially bulk medium with time-varying permittivity $\varepsilon(t)$. In the eigenmode analysis, an infinitely temporally modulated medium is considered. However, to probe the actual optical response from such a bulk time-varying medium, we study a temporal slab. We show the chosen $\varepsilon(t)$ profile of that temporal slab in Fig. 1(b). We assume that the permittivity stays at a certain constant value $\varepsilon_\mathrm{min} = 8.7$ until time t_a. Then, it changes as a function of time in the form of a rectangular wave with $\varepsilon_\mathrm{max} = 15.3$, duty cycle $d = 0.7$, and frequency $\omega_\mathrm{m} = 6 \times 10^{14}$ rads^{-1} until time t_b. Then, it returns to the constant value ε_min. Here, between time t_a and t_b, we assume nine complete cycles and one incomplete cycle of the rectangular wave. Further, N is taken as 5 (see Eq. (3c)). Note that as verified numerically, $N = 5$ leads to sufficient convergence of the solutions of Eq. (3). The corresponding homogenized setting is shown in Fig. 1(c). Here, the system

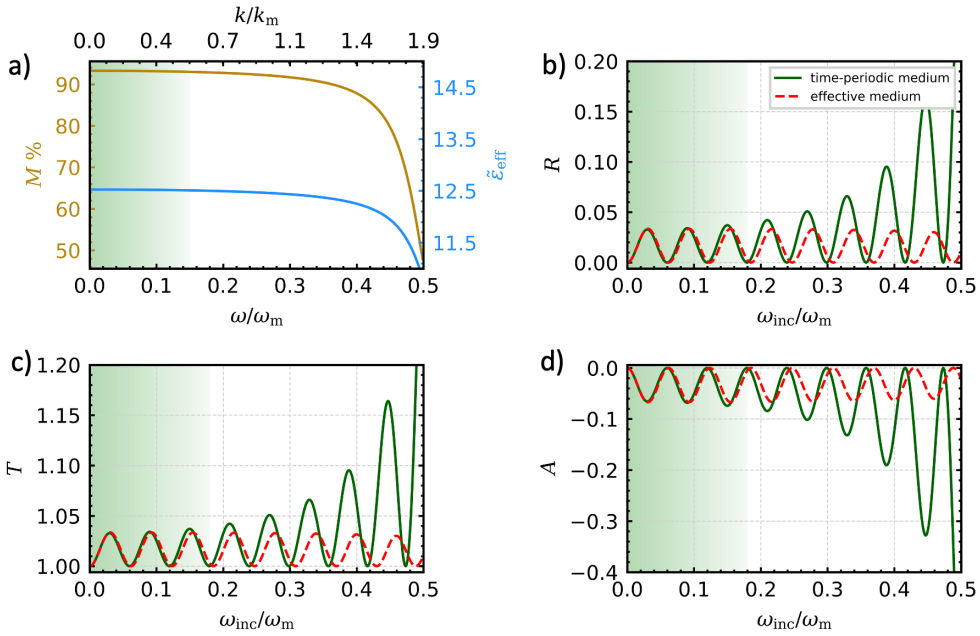

Fig. 2. a) Monochromaticity of the eigenmodes of the bulk time-periodic medium (golden curve) and effective permittivity of the corresponding homogenized medium (blue curve) as a function of the eigenfrequency ω and eigenwavenumber k. b), c), d) Comparison of reflectivity R, transmissivity T, and absorptivity A, respectively, for the time-periodic and effective media as a function of the incident frequency ω_{inc} for a temporal slab. Here, the green-shaded region represents the spectral region where the effective medium description remains valid. Further, $k_m = \omega_m/c_0$ and $\omega_{\text{inc}} = \frac{c_0 k}{\sqrt{\varepsilon_{\text{min}}}}$.

effectively behaves as a time-invariant medium with the effective permittivity $\tilde{\varepsilon}_{\text{eff}}$ between time t_a and t_b. Note that in Fig. 1(c), the homogenized system still maintains the temporal interfaces at time t_a and t_b.

As a first step, we identify the spectral region where the system in Fig. 1(b) can be homogenized. For this purpose, we solve the eigenvalue equation for the eigenvectors $\mathbf{S}_{\kappa_i}$ of an infinitely time-periodic system (see Eq. (3)). The temporal unit cell of the infinitely periodic system is taken as one period of the rectangular wave shown in Fig. 1(b) (the black-dotted lines represent the unit cell). Next, using Eq. (5), we calculate the monochromaticity $M\%$ of the eigenmodes as shown by the golden curve in Fig. 2(a). From Fig. 2(a), we observe that we can treat the time-periodic medium as quasi-monochromatic in the green-shaded spectral region. This is because, in such a spectral region, $M\%$ is sufficiently high. Numerically, $M\% \geq 92\%$ in the green-shaded spectral region. Further, the quantity Q for the eigenmodes also has a vanishing value in the green-shaded spectral region (see the Supplementary Material; Fig. S1(a)). Therefore, we use Eq. (6) to calculate the effective permittivity $\tilde{\varepsilon}_{\text{eff}}$ of the homogenized system (see Fig. 1(c)). We show the corresponding $\tilde{\varepsilon}_{\text{eff}}$ by the blue curve in Fig. 2(a). Note that the effective medium description is only valid in the green-shaded spectral region in Fig. 2(a).

Having calculated the effective permittivity $\tilde{\varepsilon}_{\text{eff}}$ of the homogenized system in Fig. 1(c), we proceed to compare the optical observables from a temporal slab made from the time-periodic system in Fig. 1(b). These optical observables are reflectivity R, transmissivity T, and absorptivity A. In Figs. 1(b)–(c), we observe the existence of temporal interfaces. At each of these temporal

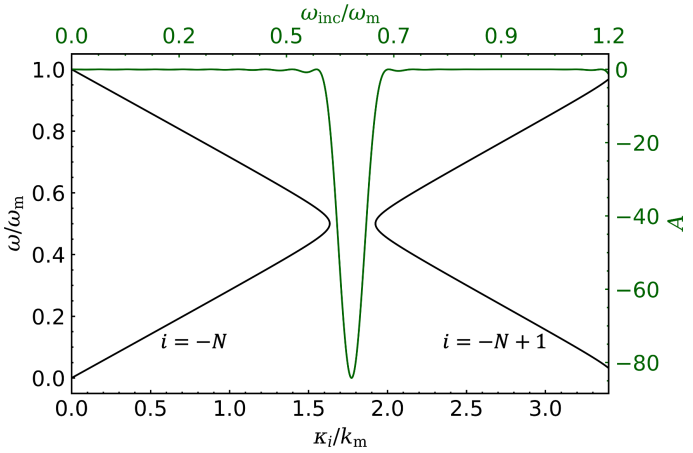

Fig. 3. Band structure of the infinitely time-periodic medium (black curve), and variation of absorptivity A of the time-periodic system shown in Fig. 1(b) as a function of the incident frequency ω_{inc} (green curve). Here, $\omega_{\mathrm{inc}} = \frac{c_0 \kappa_i}{\sqrt{\varepsilon_{\mathrm{min}}}}$.

interfaces, a monochromatic incident plane wave (PW) undergoes time reflection and time transmission [16]. Therefore, reflectivity R (transmissivity T) can be computed by analyzing the ratio of the power of the backward (forward) propagating PW after time $t = t_{\mathrm{b}}$ to the power of the incident PW before time $t = t_{\mathrm{a}}$ [54]. Moreover, absorptivity A is computed as $A = 1 - R - T$ [20]. To test our proposed method, we assume the incident PW to be $\mathbf{E}_{\mathrm{inc}}(\mathbf{r}, t) = \mathrm{e}^{\mathrm{i}(\mathbf{k}_{\mathrm{inc}} \cdot \mathbf{r} - \omega_{\mathrm{inc}} t)} \hat{\mathbf{u}}_{\mathbf{k}}$ in both media (see Figs. 1(b)–(c)). Here, $\hat{\mathbf{u}}_{\mathbf{k}}$ is a unit vector transverse to the wavevector $\mathbf{k}_{\mathrm{inc}}$. Further, the incident frequency $\omega_{\mathrm{inc}} = \frac{c_0 k_{\mathrm{inc}}}{\sqrt{\varepsilon_{\mathrm{min}}}}$, where k_{inc} is the magnitude of the wavevector $\mathbf{k}_{\mathrm{inc}}$. Note that, due to the spatial homogeneity of the considered media, $\mathbf{k}_{\mathrm{inc}}$ is conserved at all times t [61]. The conservation of $\mathbf{k}_{\mathrm{inc}}$ also holds for the temporal interfaces at $t = t_{\mathrm{a}}$ and t_{b} (see Figs. 1(b)–(c)). Therefore, to excite the quasi-monochromatic modes, we must choose $k_{\mathrm{inc}} = k$ such that k lies in the green-shaded spectral region (see Fig. 2(a)).

Next, we compare R, T, and A of both media as a function of the incident frequency ω_{inc} in Figs. 2(b)–(d). We compute these quantities using the transfer matrix approach explained in [54]. From Figs. 2(b)–(d), we observe a good agreement of the observables R, T, and A in the green-shaded spectral region. This is expected since, in such a spectral region, on the one hand, the excited eigenmodes are monochromatic (see Fig. 2(a)). On the other hand, the eigenfrequency ω lies in the first temporal BZ, i.e., $\omega < 0.5\omega_{\mathrm{m}}$ (see Subsection 2.2.2). Further, a close examination of Figs. 2(b)–(c) reveals that both the time-periodic and effective media satisfy the so-called pseudo energy conservation relation $T - R = 1$. This is expected because in both the media, the permittivity ε returns to the same value $\varepsilon_{\mathrm{min}}$ after time t_{b} as it was before the time modulation began at time t_{a} (see Figs. 1(b)–(c)). Therefore, $T - R = 1$ holds as a direct consequence of [16, Eqs. (14)–(15)].

Furthermore, from Figs. 2(b)–(d), we observe that as the ratio $\omega_{\mathrm{inc}}/\omega_{\mathrm{m}}$ increases, the agreement of R, T, and A of the time-periodic and effective media progressively worsens. The disagreement is substantial mainly outside the green-shaded spectral region. Moreover, the values of the observables R, T, and A progressively grow for the time-periodic medium as $\omega_{\mathrm{inc}}/\omega_{\mathrm{m}}$ increases. To explain these observations, we return to the infinitely time-periodic medium whose unit cell is shown by the black-dotted lines in Fig. 1(b). We plot the band structure of the infinitely time-periodic medium in Fig. 3 (with the black curve). The band structure is generated by plotting

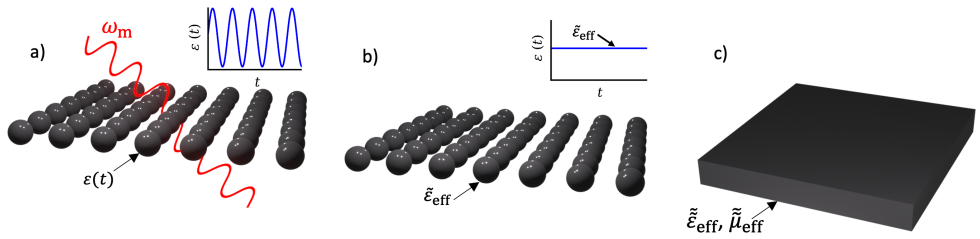

Fig. 4. a) Illustration of a spatiotemporal metasurface made from spheres. Here, each sphere has the permittivity $\varepsilon(t)$ varying as a function of time with frequency ω_m (see inset). b) Time-invariant metasurface that corresponds to the temporally homogenized system for the metasurface shown in a). Here, each sphere has the permittivity $\tilde{\varepsilon}_{eff}$ (see inset). c) Spatially uniform time-invariant slab that corresponds to the spatially homogenized medium for the system shown in b). Here, the slab is characterized by the effective permittivity $\tilde{\tilde{\varepsilon}}_{eff}$ and permeability $\tilde{\tilde{\mu}}_{eff}$.

the relationship between the eigenfrequency ω and eigenwavenumber κ_i (see Eq. (3a)). Note that, in Fig. 3, we only show the bands corresponding to the lowest and second-lowest values of κ_i, i.e., for $i = -N, -N+1$, respectively. In addition, we also plot the absorptivity A of the time-periodic system shown in Figs. 1(a)–(b) as a function of the incident frequency ω_{inc} in Fig. 3 (with the green curve). Here, ω_{inc} and κ_i are related as $\omega_{inc} = \frac{c_0 \kappa_i}{\sqrt{\varepsilon_{min}}}$. This relation holds as $k_{inc} = \kappa_i$, due to the conservation of momentum in the bulk time-varying medium.

From Fig. 3, we observe the existence of a momentum bandgap for certain κ_i values [24, 62]. Moreover, for the values of ω_{inc} which correspond to the κ_i values falling within the gap, we observe the existence of an absorption peak (R and T also show similar peaks but are omitted here for simplicity). Such growth of observables can be attributed to the momentum bandgap in Fig. 3 [63]. Furthermore, since the momentum bandgap is a feature that emerges purely because of the temporal periodicity of the system [24], the effective medium cannot capture such growth of observables. This explains the disagreement of R, T, and A for the time-periodic and effective media in Figs. 2(b)–(d) as ω_{inc}/ω_m increases.

Moreover, in Fig. 2(d), we observe that the absorptivity A is negative for both media. This is due to the power transfer between the source of temporal modulation and the modulated system [34]. Note that A is negative even for the effective medium. This is because of the power transfer occurring at the temporal interfaces at times $t = t_a$ and t_b (see Fig. 1(c)) [54].

Furthermore, we only show the agreement of reflectivity R and transmissivity T in Figs. 2(c)–(d) for the time-periodic and effective media. A similar agreement was observed for the phases of the reflection and transmission coefficients for both media. We plot these phases in the Supplementary Material; Sec 3. This also holds for the examples discussed further.

3.2. *Homogenization of spatiotemporal metasurfaces*

So far, we have discussed the homogenization of time-varying MMs that are uniform in space (see Fig. 1(a)). As the next step, we apply the proposed homogenization scheme to spatially structured time-varying (spatiotemporal) MSs.

We consider an MS made from a square lattice of dielectric spheres (see Fig. 4(a)) [20]. Each sphere in the MS is made from a material with a time-varying permittivity according to $\varepsilon(t) = 1 + \chi_{st}[1 + M_s \cos(\omega_m t)]$. Here, χ_{st} is the electrical susceptibility of the unmodulated sphere, and M_s is the modulation strength [53]. Note that such a harmonic permittivity profile is chosen for simplicity. In general, our proposed method works for any arbitrary time-periodic permittivity variation. Further, the radius of each sphere is denoted by r, and the period of the

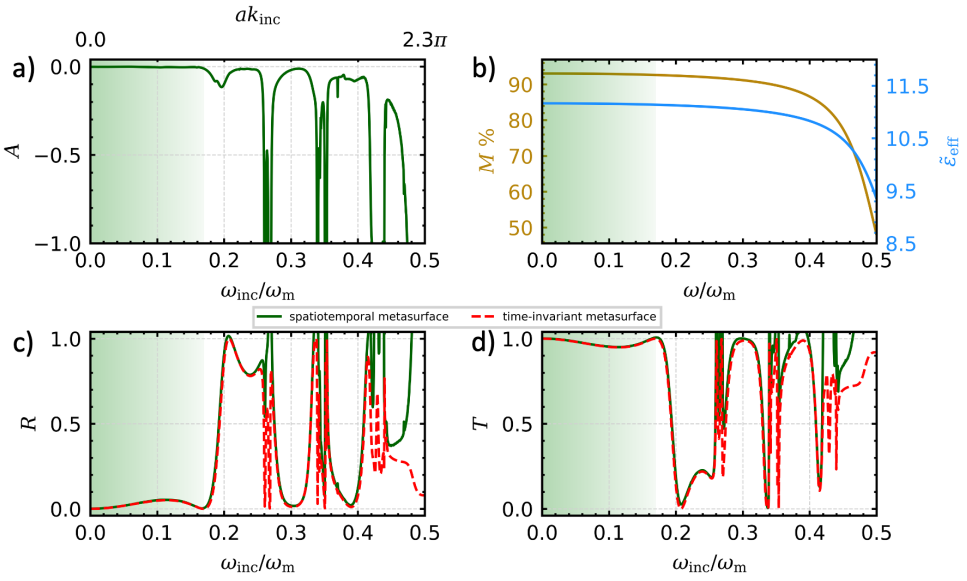

Fig. 5. a) Absorptivity A of the spatiotemporal metasurface as a function of the incident frequency ω_{inc} and the corresponding wavenumber $k_{\text{inc}}(= \omega_{\text{inc}}/c_0)$. b) Monochromaticity of the eigenmodes of the bulk time-varying medium with the same permittivity profile as the spheres in the spatiotemporal metasurface (golden curve), and correspondingly retrieved effective permittivity $\tilde{\varepsilon}_{\text{eff}}$ (blue curve) as a function of the eigenfrequency ω. c), d) comparison of reflectivity (R), and transmissivity (T), respectively, for the spatiotemporal and time-invariant but spatially structured metasurface as a function of the incident frequency ω_{inc}. Here, the green-shaded region represents the spectral region where the temporal homogenization is valid. Further, $\omega_{\text{inc}} = \omega$. Moreover, the incident plane wave impinges with the 10° incidence angle. Furthermore, it has transverse-magnetic (TM) polarization.

square lattice is denoted by a. Moreover, for simplicity, we assume the MS to be surrounded by air. To homogenize such a spatiotemporal system, we use a two-step homogenization scheme. In the first step, we approximate the optical response of the spatiotemporal MS (see Fig. 4(a)) with a time-invariant but spatially structured MS (see Fig. 4(b)). For such temporal homogenization, the method of Sec. 2 is used. Then, in the second step, we approximate the optical response of the time-invariant MS with a spatially homogeneous slab (see Fig. 4(c)). For such spatial homogenization, the well-known method of inverting the Fresnel reflection and transmission coefficients of the slab is used [6, 55].

We begin with the temporal homogenization of the spatiotemporal MS (see Figs. 4(a)–(b)). We use the T-matrix method described in [20] to numerically model the MS. In what follows, the susceptibility of the unmodulated spheres is taken to be $\chi_{\text{st}} = 11$, the radius of each sphere is $r = 800$ nm, the period of the square lattice is $a = 3r$, the modulation strength is $M_{\text{s}} = 0.4$, and the modulation frequency is $\omega_{\text{m}} = 1.8 \times 10^{15}$ rads^{-1}. Further, we assume the incident PW is the same as in the previous example, with frequency ω_{inc}. Moreover, the incident wavevector $\mathbf{k}_{\text{inc}}$ is chosen such that the angle of incidence is 10°. Furthermore, we assume the incident PW has a transverse-magnetic (TM) polarization. Note that the proposed temporal homogenization method applies to incident fields of any arbitrary angle of incidence and polarization.

To identify the spectral region where temporal homogenization is applicable, we plot the

absorptivity A of the spatiotemporal MS as a function of the incident frequency ω_{inc} in Fig. 5(a). Note that the calculation of A is done using [20, Eq. (25)]. Naturally, in the spectral region where the temporal homogenization is applicable, we expect the MS to show negligible absorptivity. This is because negative absorptivity is a feature of the temporal variance of the system. Moreover, since we are considering lossless systems, the absorptivity cannot be positive either. Therefore, in Fig. 5(a), we mark the green-shaded spectral region as the region of temporal homogenization. Note that contrary to the example of bulk time-varying media (see Fig. 1(c)), here, the homogenized structure no longer has temporal interfaces (see Fig. 4(b)). Therefore, we require negligible absorptivity of the spatiotemporal MS as a necessary condition for temporal homogenization.

Next, we retrieve the effective permittivity $\tilde{\varepsilon}_{\text{eff}}$ of the corresponding time-invariant but spatially structured MS (see Fig. 4(b)). The corresponding effective permittivity will only describe the material occupied by the spatial domain of the spheres. For such retrieval, we return to the bulk time-varying medium shown in Fig. 1(a). Note that the bulk medium has the same time-periodic permittivity $\varepsilon(t)$ as the spheres of the spatiotemporal MS shown in Fig. 4(a). Using Eq. (5), we plot the monochromaticity $M\%$ of the eigenmodes of the bulk time-varying medium in Fig. 5(b) (see the golden curve). From Fig. 5(b), we notice that in the green-shaded spectral region, the bulk eigenmodes are quasi-monochromatic as $M\%$ is sufficiently high. Numerically, $M\% \geq 92\%$ in the green-shaded spectral region. Further, the quantity Q for the eigenmodes also has a vanishing value in the green-shaded spectral region (see the Supplementary Material; Fig. S1(b)). Therefore, we use Eq. (6) to retrieve the corresponding effective permittivity $\tilde{\varepsilon}_{\text{eff}}$. We show the retrieved $\tilde{\varepsilon}_{\text{eff}}$ by the blue curve in Fig. 5(b). Note that, as required by the monochromaticity of the eigenmodes, such an effective medium description characterized by $\tilde{\varepsilon}_{\text{eff}}$ is only valid in the green-shaded spectral region shown in Fig. 5(b).

Next, we compare the optical observables (R and T) of the spatiotemporal and time-invariant but spatially structured MSs. We assume that each sphere in the time-invariant MS has permittivity $\tilde{\varepsilon}_{\text{eff}}$ (see Figs. 4(b) and 5(b)). In Figs. 5(c)–(d), we show reflectivity R and transmissivity T as a function of the incident frequency ω_{inc} for both systems. Here, the calculation of R and T is done using [20, Eqs. (23)–(24)]. Note that to excite the quasi-monochromatic eigenmode at frequency ω in the spatiotemporal MS, we must choose $\omega_{\text{inc}} = \omega$ (see Fig. 5(b)). This is because, in the limit of temporal homogenization, the spatiotemporal MS conserves the frequency of the incident field. From Figs. 5(c)–(d), we observe a good agreement of the optical observables (R and T) of both the systems in the green-shaded spectral region. This is expected, as in the low-frequency limit, i.e., $\omega_{\text{inc}}/\omega_{\text{m}} \ll 1$, the temporal variation is so fast that the incident field only sees the effective time-invariant system [49]. The observation of such good agreement is further supported by negligible absorptivity of the spatiotemporal MS in the green-shaded spectral region (see Fig. 5(a)). Moreover, in Figs. 5(c)–(d), we observe that the predictions of temporal homogenization break down as the ratio $\omega_{\text{inc}}/\omega_{\text{m}}$ increases (mainly outside the green-shaded region). This breakdown is particularly drastic at the spectral locations of the resonances of R and T. To explain this, we first note that the resonant behavior of R and T in Figs. 5(c)–(d) occurs due to the Mie resonances supported by the unmodulated spheres (with $M_{\text{s}} = 0$) of the MS shown in Fig. 4(a) [64]. See the Supplementary Material; Fig. S5 for the Mie coefficients of the unmodulated spheres. Upon temporal modulation, these Mie resonances enhance the light-matter interaction, giving rise to sharp peaks of negative absorption (see Fig. 5(a)). Naturally, these negative absorption peaks cannot be captured by the time-invariant MS. This gives rise to the disagreement of the optical response of the spatiotemporal and time-invariant MSs in Figs. 5(c)–(d).

After temporal homogenization, our system of operation is reduced to a time-invariant but spatially structured MS (see Fig. 4(b)). As evident from Fig. 5(a), we chose the lattice period a of the MS such that it is also spatially homogenizable in the green-shaded spectral region.

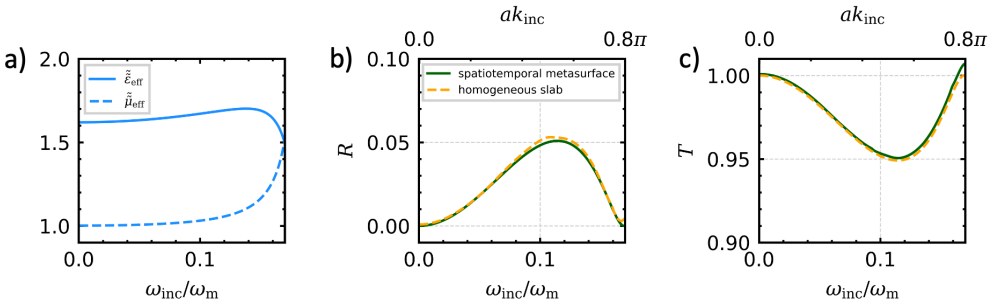

Fig. 6. a) Effective permittivity $\tilde{\tilde{\varepsilon}}_{\text{eff}}$ (solid curve), and effective permeability $\tilde{\tilde{\mu}}_{\text{eff}}$ (dotted curve) of the slab as a function of the incident frequency ω_{inc}. b), c) Comparison of reflectivity R, and transmissivity T, respectively, for the spatiotemporal metasurface and homogeneous slab as a function of the incident frequency ω_{inc} and the corresponding wavenumber k_{inc}. Note the range of ω_{inc} (and k_{inc}) shown here corresponds to the green-shaded spectral region shown in Fig. 5

Such spatial homogenizability is ensured as $ak_{\text{inc}} \ll 2\pi$ in the green-shaded region, where $k_{\text{inc}} = \omega_{\text{inc}}/c_0$ [46, 59, 60]. Therefore, we can approximate the optical response of the time-invariant MS shown in Fig. 4(b) by the slab shown in Fig. 4(c). Here, the thickness of the slab is taken as the diameter of the spheres, i.e., $2r$. Such a slab can be optically characterized by an effective permittivity $\tilde{\tilde{\varepsilon}}_{\text{eff}}$, and effective permeability $\tilde{\tilde{\mu}}_{\text{eff}}$ (see Fig. 4(c)). Further, these effective parameters of the slab can be computed by inverting the Fresnel coefficients expressing the complex reflection and transmission amplitudes from a slab [6, 55].

Therefore, after inverting the Fresnel coefficients from the slab for 10° incidence using [6, Eqs. (4)–(10)], we show its effective parameters $\tilde{\tilde{\varepsilon}}_{\text{eff}}$ and $\tilde{\tilde{\mu}}_{\text{eff}}$ in Fig. 6(a). Note that we used complex reflection and transmission coefficients of the time-invariant but spatially structured MS to perform this inversion. Further, the range of incident frequencies ω_{inc} is taken such that it lies in the green-shaded spectral region (see Fig. 5(a)). From Fig. 6(a), we observe the departure of $\tilde{\tilde{\mu}}_{\text{eff}}$ from unity for $\omega_{\text{inc}}/\omega_{\text{m}} > 0.1$. Such effective magnetic response of the slab is due to a magnetic dipolar resonance supported by the unmodulated spheres (with $M_{\text{s}} = 0$) of the MS shown in Fig. 4(a) at $\omega_{\text{inc}}/\omega_{\text{m}} = 0.18$ [4, 6, 64]. See the Supplementary Material; Fig. S5 for the Mie coefficients of the unmodulated spheres.

Next, as before, we compare the optical observables of the spatiotemporal MS with that of the slab in Figs. 6(b)–(c). From Figs. 6(b)–(c), we observe a good agreement of the observables R and T of both systems. This is expected because, to begin with, the MS is temporally homogenizable for the shown incident frequencies (see Fig. 5(a)). Further, spatial homogenizability is ensured as the incident field is such that $ak_{\text{inc}} \ll 2\pi$ [46, 59, 60]. Therefore, only the principal diffraction order of the field scattered off the MS is non-evanescent. Furthermore, in such a long wavelength limit, the first Bragg resonance of the MS is also away from the spectral region of operation. Such resonance occurs at $ak_{\text{inc}} = \pi$ [65, 66]. Therefore, the optical response of the MS can be well approximated by the slab.

4. Conclusions

We have presented an eigenmode-based approach to homogenize spatiotemporal MSs. We started with the calculation of the eigenmodes of bulk time-varying media. Then, we used these eigenmodes to retrieve the effective permittivity of the corresponding homogenized media. Next, we verified our approach by comparing the optical observables of the bulk time-varying and corresponding homogenized media. Then, we showed the applicability of our homogenization method to spatiotemporal MSs. Following a two-step homogenization scheme, we approximated

the optical response of the spatiotemporal MS with a homogeneous slab. Again, the optical observables of the spatiotemporal MS and the slab were compared to verify our method.

Our homogenization method can be applied independent of the shape of the periodic temporal modulation. A further extension of our study could include material dispersion in the temporally modulated media. Moreover, one can extend the spectral range of applicability of the homogenization method by considering the nonlocal response of the effective media.

Funding. Content in the funding section will be generated entirely from details submitted to Prism.

Acknowledgments. P.G., B.V., and C.R. gratefully acknowledge financial support by the Deutsche Forschungsgemeinschaft (DFG, German Research Foundation) through Project-ID No. 258734477 - SFB 1173. P.G., A.G.L., and C.R. are part of the Max Planck School of Photonics, supported by the Bundesministerium für Bildung und Forschung, the Max Planck Society, and the Fraunhofer Society. P.G. and A.G.L. acknowledge support from the Karlsruhe School of Optics and Photonics (KSOP). S.R. acknowledges support by the Erasmus Mundus EUROPHOTONICS M.Sc. program. The authors would like to thank Lukas Rebholz for sharing his plotting template.

Disclosures. The authors declare no conflicts of interest.

Data availability. Data underlying the results presented in this paper are not publicly available at this time but may be obtained from the authors upon reasonable request.

Supplemental document. See Supplement 1 for supporting content.

References

1. M. Kadic, G. W. Milton, M. van Hecke, and M. Wegener, "3d metamaterials," Nat. Rev. Phys. **1**, 198 (2019).
2. N. Meinzer, W. Barnes, and I. Hooper, "Plasmonic meta-atoms and metasurfaces," Nat. Photonics **8**, 889 (2014).
3. N. Zheludev and Y. Kivshar, "From metamaterials to metadevices," Nat. materials **11**, 917 (2012).
4. A. Alù, "First-principles homogenization theory for periodic metamaterials," Phys. Rev. B **84**, 075153 (2011).
5. D. R. Smith, W. J. Padilla, D. C. Vier, S. C. Nemat-Nasser, and S. Schultz, "Composite medium with simultaneously negative permeability and permittivity," Phys. Rev. Lett. **84**, 4184 (2000).
6. C. Menzel, C. Rockstuhl, T. Paul, F. Lederer, and T. Pertsch, "Retrieving effective parameters for metamaterials at oblique incidence," Phys. Rev. B **77**, 195328 (2008).
7. G. Ma and P. Sheng, "Acoustic metamaterials: From local resonances to broad horizons," Sci. Adv. **2**, e1501595 (2016).
8. R. Fleury, F. Monticone, and A. Alù, "Invisibility and cloaking: Origins, present, and future perspectives," Phys. Rev. Appl. **4**, 037001 (2015).
9. J. B. Pendry, "Negative refraction makes a perfect lens," Phys. Rev. Lett. **85**, 3966–3969 (2000).
10. S. Haxha, F. Abdelmalek, F. Ouerghi, M. Charlton, A. Aggoun, and X. Fang, "Metamaterial superlenses operating at visible wavelength for imaging applications," Sci. Reports **8**, 16119 (2018).
11. N. I. Landy, S. Sajuyigbe, J. J. Mock, D. R. Smith, and W. J. Padilla, "Perfect metamaterial absorber," Phys. Rev. Lett. **100**, 207402 (2008).
12. U. Huebner, E. Pshenay-Severin, R. Alaee, C. Menzel, M. Ziegler, C. Rockstuhl, F. Lederer, T. Pertsch, H.-G. Meyer, and J. Popp, "Exploiting extreme coupling to realize a metamaterial perfect absorber," Microelectron. Eng. **111**, 110 (2013).
13. G. Bouchitte, C. Bourel, and D. Felbacq, "Homogenization near resonances and artificial magnetism in 3d dielectric metamaterials," Arch. for Ration. Mech. Anal. **225**, 1233 (2017).
14. Y. Liu, G. Wang, J. Pendry, and S. Zhang, "All-angle reflectionless negative refraction with ideal photonic weyl metamaterials," Light. Sci. & Appl. **11**, 276 (2022).
15. J. Zhou, D. R. Chowdhury, R. Zhao, A. K. Azad, H.-T. Chen, C. M. Soukoulis, A. J. Taylor, and J. F. O'Hara, "Terahertz chiral metamaterials with giant and dynamically tunable optical activity," Phys. Rev. B **86**, 035448 (2012).
16. E. Galiffi, R. Tirole, S. Yin, H. Li, S. Vezzoli, P. Huidobro, M. Silveirinha, R. Sapienza, A. Alù, and J. Pendry, "Photonics of time-varying media," Adv. Photonics **4**, 014002 (2022).
17. Z. Hayran and F. Monticone, "Using time-varying systems to challenge fundamental limitations in electromagnetics: Overview and summary of applications," IEEE Antennas Propag. Mag. **65**, 29–38 (2023).
18. N. Engheta, "Four-dimensional optics using time-varying metamaterials," Science **379**, 1190 (2023).
19. V. Pacheco-Peña, D. M. Solís, and N. Engheta, "Time-varying electromagnetic media: opinion," Opt. Mater. Express **12**, 3829 (2022).
20. P. Garg, A. G. Lamprianidis, D. Beutel, T. Karamanos, B. Verfürth, and C. Rockstuhl, "Modeling four-dimensional metamaterials: a t-matrix approach to describe time-varying metasurfaces," Opt. Express **30**, 45832–45847 (2022).
21. H. Moussa, G. Xu, S. Yin, E. Galiffi, Y. Radi, and A. Alù, "Observation of temporal reflection and broadband frequency translation at photonic time interfaces," Nat. Phys. **19**, 863 (2023).

22. E. Lustig, O. Segal, S. Saha, E. Bordo, S. N. Chowdhury, Y. Sharabi, A. Fleischer, A. Boltasseva, O. Cohen, V. M. Shalaev, and M. Segev, "Time-refraction optics with single cycle modulation," Nanophotonics **12**, 2221 (2023).
23. M. Salehi, P. Rahmatian, M. Memarian, and K. Mehrany, "Frequency conversion in time-varying graphene microribbon arrays," Opt. Express **30**, 32061 (2022).
24. J. R. Zurita-Sánchez, P. Halevi, and J. C. Cervantes-González, "Reflection and transmission of a wave incident on a slab with a time-periodic dielectric function $\varepsilon(t)$," Phys. Rev. A **79**, 053821 (2009).
25. X. Wang, P. Garg, M. S. Mirmoosa, A. G. Lamprianidis, C. Rockstuhl, and V. S. Asadchy, "Unleashing infinite momentum bandgap using resonant material systems," arXiv preprint arXiv:2310.02786 (2023).
26. J. B. Khurgin, "Photonic time crystals and parametric amplification: similarity and distinction," (2023).
27. A. Shaltout, A. Kildishev, and V. Shalaev, "Time-varying metasurfaces and lorentz non-reciprocity," Opt. Mater. Express **5**, 2459 (2015).
28. X. Wang, V. Asadchy, S. Fan, and S. Tretyakov, "Space–time metasurfaces for power combining of waves," ACS Photonics **8**, 3034 (2021).
29. V. Pacheco-Peña and N. Engheta, "Antireflection temporal coatings," Optica **7**, 323 (2020).
30. V. Pacheco-Peña and N. Engheta, "Temporal aiming," Light. Sci. & Appl. **9**, 129 (2020).
31. N. Chamanara, S. Taravati, Z.-L. Deck-Léger, and C. Caloz, "Optical isolation based on space-time engineered asymmetric photonic band gaps," Phys. Rev. B **96**, 155409 (2017).
32. F. R. Prudêncio and M. G. Silveirinha, "Synthetic axion response with space-time crystals," Phys. Rev. Appl. **19**, 024031 (2023).
33. J. S. Martínez-Romero and P. Halevi, "Parametric resonances in a temporal photonic crystal slab," Phys. Rev. A **98**, 053852 (2018).
34. V. Asadchy, A. Lamprianidis, G. Ptitcyn, M. Albooyeh, Rituraj, T. Karamanos, R. Alaee, S. Tretyakov, C. Rockstuhl, and S. Fan, "Parametric mie resonances and directional amplification in time-modulated scatterers," Phys. Rev. Appl. **18**, 054065 (2022).
35. M. M. Sadafi, A. F. da Mota, and H. Mosallaei, "Dynamic control of light scattering in a single particle enabled by time modulation," Appl. Phys. Lett. **123**, 101702 (2023).
36. N. Stefanou, I. Stefanou, E. Almpanis, N. Papanikolaou, P. Garg, and C. Rockstuhl, "Light scattering by a periodically time-modulated object of arbitrary shape: the extended boundary condition method," J. Opt. Soc. Am. B **40**, 2842 (2023).
37. M. Z. Alam, I. De Leon, and R. W. Boyd, "Large optical nonlinearity of indium tin oxide in its epsilon-near-zero region," Science **352**, 795 (2016).
38. J. Bohn, T. S. Luk, S. Horsley, and E. Hendry, "Spatiotemporal refraction of light in an epsilon-near-zero indium tin oxide layer: frequency shifting effects arising from interfaces," Optica **8**, 1532 (2021).
39. M. Lobet, N. Kinsey, I. Liberal, H. Caglayan, P. A. Huidobro, E. Galiffi, J. R. Mejía-Salazar, G. Palermo, Z. Jacob, and N. Maccaferri, "New horizons in near-zero refractive index photonics and hyperbolic metamaterials," (2023).
40. S. Saha, O. Segal, C. Fruhling, E. Lustig, M. Segev, A. Boltasseva, and V. M. Shalaev, "Photonic time crystals: a materials perspective," Opt. Express **31**, 8267 (2023).
41. V. Pacheco-Peña and N. Engheta, "Merging effective medium concepts of spatial and temporal media: Opening new avenues for manipulating wave-matter interaction in 4d," IEEE Antennas Propag. Mag. **65**, 39–49 (2023).
42. P. Huidobro, M. Silveirinha, E. Galiffi, and J. Pendry, "Homogenization theory of space-time metamaterials," Phys. Rev. Appl. **16**, 014044 (2021).
43. J. C. Serra and M. G. Silveirinha, "Homogenization of dispersive space-time crystals: Anomalous dispersion and negative stored energy," Phys. Rev. B **108**, 035119 (2023).
44. M. Kreiczer and Y. Hadad, "Wave analysis and homogenization of a spatiotemporally modulated wire medium," Phys. Rev. Appl. **16**, 054003 (2021).
45. D. R. Smith and J. B. Pendry, "Homogenization of metamaterials by field averaging (invited paper)," J. Opt. Soc. Am. B **23**, 391 (2006).
46. R. Venkitakrishnan, T. Höß, T. Repän, F. Z. Goffi, M. Plum, and C. Rockstuhl, "Lower limits for the homogenization of periodic metamaterials made from electric dipolar scatterers," Phys. Rev. B **103**, 195425 (2021).
47. V. Pacheco-Peña and N. Engheta, "Effective medium concept in temporal metamaterials," Nanophotonics **9**, 379 (2020).
48. X. Zhu, H.-W. Wu, Y. Zhuo, Z. Liu, and J. Li, "Effective medium for time-varying frequency-dispersive acoustic metamaterials," Phys. Rev. B **108**, 104303 (2023).
49. D. Torrent, "Strong spatial dispersion in time-modulated dielectric media," Phys. Rev. B **102**, 214202 (2020).
50. C. Rizza, G. Castaldi, and V. Galdi, "Nonlocal effects in temporal metamaterials," Nanophotonics **11**, 1285 (2022).
51. E. Panagiotidis, E. Almpanis, N. Papanikolaou, and N. Stefanou, "Inelastic light scattering from a dielectric sphere with a time-varying radius," Phys. Rev. Appl. **106**, 013524 (2022).
52. X. Wang, M. S. Mirmoosa, V. S. Asadchy, C. Rockstuhl, S. Fan, and S. A. Tretyakov, "Metasurface-based realization of photonic time crystals," Sci. Adv. **9**, eadg7541 (2023).
53. G. Ptitcyn, A. Lamprianidis, T. Karamanos, V. Asadchy, R. Alaee, M. Müller, M. Albooyeh, M. S. Mirmoosa, S. Fan, S. Tretyakov, and C. Rockstuhl, "Floquet–mie theory for time-varying dispersive spheres," Laser & Photonics Rev. **17**, 2100683 (2023).
54. D. Ramaccia, A. Alù, A. Toscano, and F. Bilotti, "Temporal multilayer structures for designing higher-order transfer

functions using time-varying metamaterials," Appl. Phys. Lett. **118**, 101901 (2021).
55. D. R. Smith, S. Schultz, P. Markoš, and C. M. Soukoulis, "Determination of effective permittivity and permeability of metamaterials from reflection and transmission coefficients," Phys. Rev. B **65**, 195104 (2002).
56. Note that we define the Fourier transform $\tilde{f}(\omega)$ of a time-dependent function $f(t)$ as $\tilde{f}(\omega) = \frac{1}{\sqrt{2\pi}} \int_{-\infty}^{\infty} f(t) e^{i\omega t} \mathrm{d}\omega$.
57. P. Moon and D. E. Spencer, *The Vector Helmholtz Equation* (Springer Berlin Heidelberg, Berlin, Heidelberg, 1961), p. 136.
58. S. A. R. Horsley, E. Galiffi, and Y.-T. Wang, "Eigenpulses of dispersive time-varying media," Phys. Rev. Lett. **130**, 203803 (2023).
59. H. Nassar, Q.-C. He, and N. Auffray, "Willis elastodynamic homogenization theory revisited for periodic media," J. Mech. Phys. Solids **77**, 158 (2015).
60. H. Nassar, "Elastodynamic homogenization of periodic media," Theses, Université Paris-Est (2015).
61. A. Ortega-Gomez, M. Lobet, J. E. Vázquez-Lozano, and I. nigo Liberal, "Tutorial on the conservation of momentum in photonic time-varying media [invited]," Opt. Mater. Express **13**, 1598–1608 (2023).
62. S. Sadhukhan and S. Ghosh, "Momentum controlled optical pulse amplification in photonic time crystals," (2023).
63. J. Gaxiola-Luna and P. Halevi, "Growing fields in a temporal photonic (time) crystal with a square profile of the permittivity ε (t)," Appl. Phys. Lett. **122**, 011702 (2023).
64. A. Rahimzadegan, R. Alaee, C. Rockstuhl, and R. W. Boyd, "Minimalist mie coefficient model," Opt. Express **28**, 16511–16525 (2020).
65. M. Rybin, D. Filonov, K. Samusev, P. Belov, Y. Kivshar, and M. Limonov, "Phase diagram for the transition from photonic crystals to dielectric metamaterials," Nat. Commun. **6** (2015).
66. B. Zerulla, R. Venkitakrishnan, D. Beutel, M. Krstić, C. Holzer, C. Rockstuhl, and I. Fernandez-Corbaton, "A t-matrix based approach to homogenize artificial materials," Adv. Opt. Mater. **11**, 2201564 (2023).